

1 **Analysis of the crystallization process of a**
2 **biopharmaceutical compound in the presence of**
3 **impurities using process analytical technology**
4 **(PAT) tools**

5 Elena Simone,¹ Wei Zhang,^{2,3} Zoltan K. Nagy*^{1,3}

6

7 *¹ Department of Chemical Engineering, Loughborough University, Loughborough, LE11*
8 *3TU, U.K.*

9 *² New drug research and development center, North China Pharmaceutical group*
10 *Corporation, Shijiazhuang, China*

11 *³ School of Chemical Engineering, Purdue University, West Lafayette, 47907, Indiana,*
12 *United State*

13

1 **Abstract**

2 The crystallization of biopharmaceuticals can be problematic since, because the biosynthesis
3 of these compounds is very difficult to control, they can present a significant amount of
4 impurities that has to be eliminated. In fact, impurities can lead to changes in the properties of
5 the drug that can significantly reduce its effectiveness or even put in danger the user.

6 The substance used in this work is vitamin B12 crude product extracted from fermentation.

7 The aim of this work is to exploit process analytical technology (PAT) tools to study the
8 crystallization step of vitamin B12. Linear cooling crystallization experiments were
9 performed using different conditions. The effects of solvent, cooling rate, seeding and purity
10 of the initial material on the final size distribution and purity of the crystals were investigated
11 through the use of UV/Vis spectroscopy, focused beam reflectance measurement (FBRM)
12 and the CryPRINS software (Crystallization Process Informatics System).

13 It was found that impurities strongly inhibit the growth of vitamin B12 crystals, promoting
14 nucleation and leading to a poor final crystal size distribution. Slow cooling can help in
15 increasing the purity of the final product but also generates a broad crystal size distribution
16 because of secondary nucleation. Preparing the solution with material already crystallized
17 once and using purified seeds helped in obtaining a narrower crystal size distribution and also
18 reduces breakage.

19

20 **Keywords:** PAT tools, biopharmaceutical, vitamin, crystallization, monitoring

21

1 **Introduction**

2 Over the last decade the investment in research and development of biopharmaceutical
3 companies has more than doubled: there is a great interest in formulating and optimizing the
4 manufacturing of bio-molecules and biopharmaceuticals such as proteins, lipids, vitamins,
5 hormones and DNA. Those compounds can be used in the treatment of serious diseases or
6 just as nutritional supplement.

7 Vitamin B12 (cobalamin) is one of the biggest and most complex vitamins and, in humans, it
8 is required to assist the actions of two enzymes: methionine synthase and (R)-methylmalonyl-
9 CoA mutase. It is commonly used to cure pernicious anemia and its deficiency determines an
10 increase in homocysteine levels that leads to a major risk for heart disease, stroke,
11 atherosclerosis and vascular diseases. Despite the lack of solid evidences on the importance
12 of vitamin B12 in maintaining normal myelination of nerve cells, its role in preventing many
13 neurological and psychiatric symptoms is becoming clearer and clearer. For these reasons,
14 every year, around 10 tons of the semisynthetic version of vitamin B12 (cyanocobalamin) are
15 produced by biofermentation from several bacterial species.¹

16 A schematic of vitamin B12 molecule is shown in Figure 1. The molecule is fairly large and
17 complex and can be divided in three parts: (1) a central corrin ring which contains four
18 ligands for the central cobalt ion, (2) a lower ligand donated by the 5,6-
19 dimethylbenzimidazole (DMBI) and (3) an upper ligand made from either an adenosyl group
20 or a methyl group.

21 Two pseudo-polymorphic forms were discovered by X-ray diffraction: a wet and a dry
22 crystalline structure.^{2,3} The main difference between the two is the presence of water
23 molecules in the crystal lattice that makes the unit cell of the wet form bigger than the dry.
24 Cyanocobalamin is mainly produced by biosynthetic fermentation processes, although a full
25 chemical synthesis (consisting of 70 steps) was developed in the early 70s.¹ High levels of

1 impurities are present in the biosynthesized vitamin B12 that can inhibit growth of the
2 crystals and strongly affect the final crystal size distribution together with the ease of
3 downstream processes (filtration in particular).

4 Process analytical technology (PAT) tools are widely used for the development of the
5 crystallization processes of many synthetic pharmaceuticals.⁴⁻⁶ The term PAT refers to “a
6 system for designing, analyzing, and controlling manufacturing through timely measurement
7 of critical quality and performance attributes of raw and in-process material and processes,
8 with the goal of ensuring final product quality”.⁷ PAT tools are the main element used in the
9 “Quality by Design” (QbD) approach that was introduced in the pharmaceutical industries in
10 order to minimize product waste due to mistakes in the manufacturing process. The QbD
11 concept consists in obtaining the desired quality of the product through the correct design of
12 the manufacturing process. In this approach some critical variables of the process, strictly
13 related to the quality of the product, are controlled during the manufacturing in order to
14 control the quality of the product itself.^{8,9} The QbD approach is well known and applied in
15 the pharmaceutical industry but only few examples are present for the manufacturing of
16 biopharmaceuticals.^{10,11} Despite the difficulty of controlling biological processes Near
17 infrared (NIR) and Raman spectroscopy, HPLC and image analysis were recently used for
18 some manufacturing steps of biomolecules.¹²⁻¹⁴

19 In this work the crystallization of vitamin B12 will be studied with PAT tools (ATR-UV/Vis,
20 FBRM and CryPRINS) and the effect of impurities on the growth and nucleation rate will be
21 analyzed. The produced crystals are analyzed with optical microscopy, HPLC and Raman.
22 Most of the impurities in cyanocobalamin have high levels of fluorescence and, therefore,
23 Raman can give an indication of the purity of the crystals since it is highly sensitive to this
24 phenomenon.^{15,16} However, for a precise quantification of the type and level of impurity in
25 vitamin B12 samples HPLC is necessary. The paper provides one of the first comprehensive

1 case studies that illustrate how an array of PAT tools can be used for the systematic
2 understanding and design of a biopharmaceutical crystallization process.

3

4 **Materials and methods**

5 *Equipment*

6 Crude Vitamin B12 produced by fermentation was donated by Hebei Welcome
7 Pharmaceutical Co., LTD (China). The raw material consisted in a dry powder containing
8 around 7% of impurities. Those were mainly byproducts of the fermentation process (e.g. 50-
9 carboxyl cyanocobalamin, 34-methyl cobalamin, 8-epi-cyanocobalamin and
10 cyanocobalaminic lactate) and inert. Ultrapure water was obtained via a Millipore ultra-pure
11 water system while ethanol was purchased by Fisher Scientific (purity >95% v/v). Pure water
12 or solutions of water and ethanol were used as solvents for the experiments.

13 Experiments were conducted at both Loughborough University, UK and Purdue University,
14 USA with similar, but not exactly identical instruments. Two 500 ml glass jacketed vessels
15 and the same Raman system (an RXN1 Raman analyzer with immersion probe and 785 nm
16 laser, Kaiser with iC Raman 4.1 software) were used. A simple schematic of the rig used for
17 the experiments is shown in Figure 2. The experiments at Loughborough University were
18 performed using an MSC621 Carl Zeiss ATR-UV/Vis spectrophotometer with Hellma ATR
19 (type 661.822-UV) probe and a LabView based in-house software, a D600L Lasentec FBRM
20 probe (Mettler Toledo with FBRM software V 6.7.0) and a Huber Ministat CC3
21 thermoregulator. The data from the FBRM, ATR-UV/Vis and the Huber is transmitted in
22 real-time to the CryPRINS software (Crystallization Process Informatics System). This
23 allows real-time monitoring and control of the FBRM counts, ATR-UV/Vis signal and the
24 temperature, as well as setting a temperature profile and performing different control
25 strategies. The instrumentation at Purdue University consisted in a Zeiss MCS621 UV/Vis

1 spectrophotometer with UV-VIS 190-720 nm Zeiss probe (Zeiss ProcessXplorer software
2 version 1,3-Build 1.3.1.30), an FBRM G400 0.5-2000microns (Mettler Toledo with ic.FBRM
3 software version 4.3) and a JULABO F25-ME thermoregulator. The samples of vitamin
4 produced were analyzed using a Raman RXN1 microprobe (Kaiser) and an HPLC Agilent
5 1100 series (Hewlett Packard) with ChemStation software rev. A.09.03[1417].

6 *Procedure for linear cooling experiments*

7 Mixtures of water and ethanol and pure water were used as solvents for the linear cooling
8 experiments. The concentrations used were about 0.118-0.13 g/g solvent in water and ethanol
9 (saturation temperature of about 50 °C) and between 0.09 and 0.11 g/g solvent for water
10 (saturation temperature of about 60 °C). The material was dissolved and the hot solution was
11 filtered (using a filter paper) before starting the cooling profile because of the presence of
12 insoluble particles in the raw material. The solubility of vitamin B12 in water at different
13 temperatures was provided by the supplying company and is shown in Table 1, while data for
14 ethanol/water mixtures at different temperatures was not available from the literature and the
15 amount of material donated was too small to accurately measure it. However, two inferential
16 curves of the solubility expressed as UV signal (absorbance value at 361 nm) were obtained
17 in order to compare two solvents. Those curves can also be directly compared with the UV
18 data in the Results and Discussion section (which is actually an absorbance and not a
19 concentration value). The curves were acquired by slow heating (0.075 °C/min) of two
20 slurries of vitamin B12 in water and ethanol/water. The amount of vitamin dissolved at any
21 time and temperature is proportional to the absorbance value recorded. Figure 3 shows the
22 inferential curves as well as the exact solubility in the two solvents at high temperatures (120
23 g/L ethanol/water solution at 53 °C, and 84 g/L water at 62 °C). The material was added to
24 the solvent at ambient temperature and then dissolved by heating the solution and keeping it
25 at high temperature for 15-20 min. In ethanol and water the higher temperature was around

1 75 °C while in pure water it was around 70 °C. Four cooling rates were used: -0.075, -0.1, -
2 0.5 and -1 °C/min (slower, slow, fast and faster cooling), both seeded and unseeded
3 experiments were performed. The cooling rates were chosen based on experience with similar
4 types of crystals, equipment and scale.¹⁹⁻²¹ The final temperature after cooling was 5-6 °C. In
5 the case of the seeded experiments the mass of seeds was of about 2.5 % of the total solid
6 dissolved in the vessel. Seeds were obtained after three successive crystallizations of the raw
7 material. The same seeds were used for all the seeded experiments: crystals were in the form
8 of short needles with fairly homogenous width (around 40-60 µm) and variable length (up to
9 around 200 µm). At the end of the profile, the temperature was kept constant for few hours
10 (until both FBRM and ATR-UV/Vis signals stabilized); after that, crystals were filtered and
11 washed with acetone. CryPRINS was used to select the desired heating/cooling rate and to
12 monitor the UV and FBRM signals during the experiments. In addition to the linear cooling
13 experiments, three consecutive crystallizations of the same material were conducted using
14 ethanol and water or pure water as solvents. Recrystallizing the same material more than once
15 allows obtaining very pure crystals but the overall yield of the process is penalized. These
16 three experiments were conducted to check the purity that could be obtained by using
17 multiple steps of crystallization compared to a single linear cooling profile. Table 2 shows the
18 conditions of the experiments performed in this section.

19 *HPLC analysis*

20 The mobile phase for the HPLC analyses was prepared dissolving 7.4 g of $Na_2HPO_4 \cdot 2H_2O$
21 (HPLC purity grade, Fisher Scientific) in 740 ml of deionized water (from a Millipore Elix 5)
22 and then adding 260 ml of methanol (Fisher Scientific). The solution pH was adjusted to 3.5
23 using H_3PO_4 (Fisons analytical reagents). The solid samples were dissolved in purified water
24 (concentration of about 1 mg/ml). For the detection of the sample constituents the UV
25 wavelength at 351 nm was used. The flow rate applied was 0.8 ml/min for a total running

1 time of 40 min for each sample. The temperature of the column was kept constant at 35 °C
2 and the injection size was 20 µl. The type of column used was an Analytical Column Waters
3 Spherisorb® 5µm C8 4.6×250 mm. The main peak at about 14 min corresponds to
4 cyanocobalamin while the other peaks are byproducts (50-carboxyl cyanocobalamin, 34-
5 methyl cobalamin, 8-Epi- cyanocobalamin, 7β,8β-cyanocobalamin lactate) and other
6 unspecified impurities. All samples were analyzed at least twice and purity was calculated as
7 the average relative area of the cyanocobalamin peak.

8 *Principal component analysis on Raman spectroscopic data*

9 Principal components analysis (PCA) is a dimension reduction technique for quantitative
10 data. Given a set of data in more variables, with PCA it is possible to reduce the dimensions
11 of the problem down to two or three, keeping at the same time, enough information to capture
12 the inherent variability within the data. PCA is a method that models all the variations in the
13 data set using orthogonal basis vectors (eigenvectors) which are called principal components
14 in this analysis.¹⁷ If A is the $n \times m$ matrix of input data (n rows of spectra recorded at m
15 wavelengths for example), PCA can decompose it in the following linear system:

$$16 \quad A = CP^T + \varepsilon, \quad (1)$$

17 where C is the $n \times k$ matrix of k principal components' scores and P is the $m \times k$ matrix
18 of the eigenvectors of A . The eigenvectors are called "loadings" in PCA. ε is a matrix
19 containing the unexplained variance. Loadings and score for PCA can be used to interpret the
20 data. The scores are usually represented in two-dimensional scatter plots. Often, a very high
21 percentage of variability is gathered in the first few principal components so only a few of
22 these plots are necessary. The scores plots are usually used to detect similarities, differences
23 or other interesting relationships among samples. A PCA was performed over Raman
24 spectroscopic data of vitamin B12 in order to determine a relation between the purity of the

1 analyzed crystals and their Raman spectra. Matlab 2013a was used for the calculation of the
2 principal component scores (*pca* function).

3

4 **Results and discussion**

5 *Linear cooling experiments*

6 Simple linear cooling was applied to the raw and recrystallized vitamin B12 and the results
7 were studied using FBRM and images from an optical microscope. The crystal size
8 distribution (CSD) was found to be strongly affected by the purity of the material used and
9 the cooling rate. Usually large crystals and a narrow crystal size distribution are preferred
10 because they facilitate the downstream operations (such as filtration, washing and milling).
11 For this reason a good quality CSD is characterized by large crystals of similar size. The
12 solvent used did not have a significant effect on the CSD but it affects the final purity of the
13 crystals. The effect of seeding was also analyzed and it was found that a slightly purer
14 material can be obtained at the end of the crystallization using purified seed. Figure 4 shows
15 the results of experiment 1 and experiment 2 described in Table 2, in which raw vitamin B12
16 was crystallized from an ethanol/water mixture at two different cooling rates (-0.5 and -
17 0.1 °C/min, fast and slow cooling). From the microscopic images of crystals at the end of the
18 two experiments (see Figure 4a and Figure 4b) it can be noticed that in both cases the size
19 distributions look very broad with both small and large crystals; but a considerably larger size
20 is clearly generated by the slow cooling shown in Figure 4b. This behaviour is similar to what
21 normally happens for common pharmaceuticals such as paracetamol.¹⁸⁻²¹ In general, during a
22 fast cooling experiment, nucleation happens at high supersaturation generating a large amount
23 of small nuclei while in a slow cooling experiment, few nuclei are nucleated at low
24 supersaturation. However, for paracetamol, a fast cooling generates a high number of total counts
25 from the FBRM due to the large number of nuclei generated at high supersaturation. In the

1 case of Vitamin B12 the trend seems to be the opposite, as shown in Figure 5a and b. In
2 experiment 1 (Figure 5a) when slow cooling was used, the number of counts was lower than
3 in experiment 2 (Figure 5b) which was conducted at a fast cooling rate. Furthermore, the
4 images from the microscope seem to contrast with the data from FBRM data since, clearly
5 less and bigger particles were generated using slow cooling (Figure 4b) compared to fast
6 cooling (Figure 4a). Additionally, the final square weighted mean chord length distribution is
7 higher for the fast cooling rate (Figure 5a) than the slow one (Figure 5b). This discrepancy
8 between images and FBRM data is related to the needle shape of the vitamin B12 crystals. As
9 the particles grow in length, the shorter size of the crystals is counted by the FBRM more
10 times than the longer giving the erroneous larger number of counts for small crystal size
11 present in the vessel. A similar behavior for this probe was observed by Leyssens et al. for a
12 small needle-like molecule prodrug antagonist called CDP323-2.²²

13 The longer the crystals are, the higher is the value of the total counts recorded by FBRM; and
14 that is the reason why slow cooling of raw vitamin B12 generated a higher value of the total
15 counts than fast cooling (70,600 #/meas. in the slow cooling against 44,000 #/meas. as shown
16 in Figure 4a and 4b). However, considering the large amount of small crystals present at the
17 end of both experiments (in particular see Figure 4a for experiment 1 and Figure 4c for
18 experiment 3), it is clear that secondary nucleation prevails on growth for raw vitamin B12.
19 This can be explained by the fact that the presence of impurities inhibits growth, and
20 supersaturation is used mainly to nucleate new small crystals.

21 Some breakage is also present in the slow cooling after 400 min as shown in the CLD
22 distribution of Figure 5d, where a reduction in the number of larger particles can be observed.
23 Breakage of crystals also contributed to the higher number of counts in the case of slow
24 cooling. Figure 6a and 6c show the FBRM and UV data for fast and slow cooling
25 crystallization of a purified solution of vitamin B12 (experiment 3 and 4 of Table 2). The use

1 of recrystallized material with fewer impurities reduced considerably both primary and
2 secondary nucleation during the cooling phase and promoted growth of the existing crystals.
3 Figure 6b and 6d show the microscopic images of the resulting crystals; the crystal size
4 distribution is narrower compared to experiment 1 and 2 and crystals are considerably larger
5 with the maximum total counts that reaches only 5,200 #/meas. in the fast cooling experiment
6 and 26,900#/meas. for the slow cooling. The effect of the shape of the crystals on the FBRM
7 data is clearer in these two experiments because of the absence of breakage or secondary
8 nucleation; crystals in Figure 6d are clearly longer than the ones shown in Figure 6b and the
9 CLD (Figure 7a and 7b) present a bimodal shape with a growing peak at low sizes due to the
10 increasing counts of the shorter size of the crystals.

11 It is clear that growth of vitamin B12 is strongly inhibited by impurities and very broad
12 crystal size distributions are generated by secondary nucleation and breakage. Additionally,
13 in some cases, multiple nucleation events can happen as shown in Figure 8b, c and d, which
14 is also a clear indication of growth inhibited crystallization processes in the presence of
15 impurities. Figure 8a shows the results for experiment 5 (Table 2) where vitamin B12
16 nucleated and grew throughout the entire cooling period. Figure 8b, 8c and 8d instead, show
17 cases in which a second major nucleation event happened during the cooling phase. The UV
18 signal dropped suddenly during the second nucleation and the counts increased at the same
19 time. This phenomenon appeared with both raw and recrystallized material, for seeded and
20 unseeded experiments and for both the solvents used. During these experiments growth was
21 so inhibited that supersaturation accumulated during the cooling until it reached a level at
22 which a second major nucleation event could happen. In these cases the final CLD is very
23 broad and many small particles are present as a result of this double nucleation as shown in
24 Figure 9 (for experiment 7).

25

1 *Purity analysis using HPLC and Raman spectroscopy*

2 A first qualitative screening of both the raw material and the crystals obtained by consecutive
3 crystallizations (with increasing purity as shown in Table 3) was performed using Raman
4 microscopy. The inert material filtered during the crystallizations was also analyzed. Figure
5 10a shows the Raman spectra of raw and filtered material; a strong fluorescence, due to
6 impurities can be noticed (high intensity and no defined peaks). It is interesting to observe
7 that just the filtration of the hot solution eliminates part of the fluorescent material. A loss of
8 fluorescence due to less impurity can also be noticed in the samples of the consecutive
9 crystallizations (Figure 10b). The number and position of the peaks is the same for all the
10 samples but they tend to become broader and less intense as fluorescence (and, therefore
11 impurity) increases. In order to have some quantitative information from Raman spectroscopy
12 a principal component analysis was performed over the Raman spectra of the recrystallized
13 material, the raw material and the filtered one. Figure 11a shows the score of principal
14 component PC2 plotted versus the score of principal component PC1. The raw and filtered
15 material points are isolated and very far from the crystallized samples because of their high
16 impurity content. Figure 11b shows only the crystallized samples: a clear trend of the scores
17 as a function of purity is present. This example provides an illustration for the non-
18 conventional use of Raman spectroscopy for monitoring low concentration of impurities
19 based on fluoresce. While fluorescence is in general undesirable in Raman spectroscopy,
20 since it makes the interpretation of the significant peaks difficult, monitoring the amount of
21 fluorescence in the Raman spectra can serve as a method of detecting the existence and
22 changes in impurity levels in the case of fluorescent impurities.

23 The loss of impurity during the consecutive crystallizations also considerably improved the
24 size of the crystals as shown in Figure 12. The raw material showed in Figure 12a is highly
25 fluorescent and amorphous; particles are very small and hygroscopic and the colour is intense

1 red. Crystalline vitamin B12 is darker as shown in Figure 12b to 12d. The mean size of the
2 crystals increases during the consecutive crystallization as a result of less inhibited growth.
3 The results of HPLC analyses of the samples from selected experiments out of those
4 performed are shown in Table 3. A higher purity can be reached if slow cooling rates are
5 applied and seeding also helps in increasing the purification efficiency. The largest increase
6 in purity was reached using raw material in an ethanol/water mixture with seeding and slow
7 cooling (linear cooling experiment 14, increase in purity of 3.65%). The second
8 crystallizations (using purified material) as expected present a lower increase in purity;
9 however, even for this set of experiments, slow cooling and seeding helped reaching a higher
10 purity. The effect of the solvent on the final crystal size distribution is negligible but choosing
11 the suitable solvent seems to help increasing the purity of the product. It also seems not to
12 affect purification efficiency since the final purity of similar experiments in different solvents
13 is very close.

14

15 **Conclusions**

16 A set of PAT tools was used to study the crystallization in the presence of impurities of a
17 small biomolecule produced by fermentation (vitamin B12). Materials produced by
18 biosynthesis often contain a high amount of impurities that can significantly reduce the
19 quality of the final crystals in term of size distribution. Multiple successive recrystallizations
20 of the same material can help eliminating impurities and reaching a better crystal size
21 distribution, but they also contribute to decrease the yield. Using PAT tools can help
22 understanding the characteristics of the studied compound and developing a correct
23 crystallization strategy to improve crystal size and purity of the final product.

24 It was found that impurities strongly affect the growth rate, promoting nucleation and, in
25 some cases, generating multiple nucleation events during the cooling profile. The final crystal

1 size distribution for these cases was found to be very broad, with very large crystals together
2 with significant amounts of fines. Slow cooling of very impure material increases the
3 probability of multiple nucleation events and, therefore, leads to a broad crystal size
4 distribution. However, slow cooling was found to generate more pure crystals compared to
5 fast cooling. The best quality of the crystals, in terms of size, was reached using already
6 crystallized material to prepare the solution and slow cooling rates. Seeding was also found to
7 help in increasing the purity of the final crystal while a change in the solvent composition did
8 not largely affect purity or final CSD. The needle shape of the vitamin B12 crystals also had
9 to be considered before interpreting the FBRM results. The growth of the long size of the
10 needles generates an increase in the FBRM total counts that can be confused with nucleation.
11 An analysis of the crystals with the optical microscope was necessary to interpret the counts
12 and chord length distribution recorded by the FBRM. Monitoring the level of fluorescence
13 due to impurities in the Raman spectrum, can serve as a method of detecting changes in the
14 impurity concentrations in the crystalized products.

15

16 **Acknowledgments**

17 Financial support provided by the European Research Council grant no. [280106-CrySys].

18 The authors are grateful to Hebei Welcome Pharmaceutical Co., LTD (China), for donating

19 vitamin B12.

1 **References**

- 2 1. Martens, J.H., Barg, H., Warren, M.J., Jahn, D., Microbial production of vitamin B12.
3 Appl Microbiol Biotechnol 58: 275-285 (2002).
- 4 2. Hodgkin, D.C., Kamper, J., Mackay, M., Pickworth, J., Structure of vitamin B12. Nature
5 178: 64-66 (1956).
- 6 3. Hodgkin, D.C., Pickworth, J., Robertson, J.H., Trueblood, K.N., Prosen, R.J., White, J.G.,
7 Structure of vitamin B12. Nature 4477: 325-328 (1955).
- 8 4. Nagy, Z.K., Braatz, R., Advances and new directions in crystallization control. Annu. Rev
9 Chem Biomol Eng, 3: 55-75 (2012).
- 10 5. Nagy, Z.K., Fevotte, G., Kramer, H., Simon, L.L., Recent advances in the monitoring,
11 modelling and control of crystallization systems. Chem Eng Res Des 91(10): 1903–1922
12 (2013).
- 13 6. Simon, L.L., Pataki, H., Marosi, G., Meemken, F., Hungerbühler, K., Baiker, A., Tummala,
14 S., Glennon, B., Kuentz, M., Steele, G., Kramer, H.J.M., Rydzak, J.W., Chen, Z., Morris,
15 J., Kjell, F., Singh, R., Gani, R., Gernaey, K.V., Louhi-Kultanen, M., O'Reilly, J.,
16 Sandler, N., Antikainen, J., Yliruusi, J., Frohberg, P., Ulrich, J., Braatz, R.D., Leyssens,
17 T., von Stosch, M., Oliveira, R., Tan, R.B.H., Wu, H., Khan, M., O'Grady, D., Pandey,
18 A., Westra, R., Delle-Case, E., Pape, D., Angelosante, D., Maret, Y., Steiger, O., Lenner,
19 M., Abbou-Oucherif, K., Nagy, Z.K., Litster, J. D., Krishna Kamaraju, V., Chiu, M.S.,
20 Assessment of Recent Process Analytical Technology (PAT) Trends: A Multiauthor
21 Review. Org Process Res Dev 19(1): 3-62 (2015).

- 1 7. Department of Health and Human Services, Food and Drug administration, PAT Guidance
2 for Industry: A Framework for Innovative Pharmaceutical Development, Manufacturing
3 and Quality Assurance. Rockville, MD (2004).
- 4 8. Rathore, A.S., Bhambure, R., Ghare, V., Process analytical technology (PAT) for
5 biopharmaceutical products. *Anal Bioanal Chem* 398: 137-154 (2010).
- 6 9. Rathore, A.S., Winkle, H., Quality by design for biopharmaceuticals. *Nature Biotechnol*
7 27(1): 26-34 (2009).
- 8 10. Read, E.K., Shah, R.B., Riley, B.S., Park, J.T., Brorson, K.A., Rathore, A.S., Process
9 Analytical Technology (PAT) for biopharmaceutical products: Part II. Concepts and
10 applications. *Biotechnol Bioengi* 105(2): 285-295 (2010).
- 11 11. Glassey, J., Gernaey, K.V., Clemens, C., Schulz, T.W., Oliveira, R., Striedner, G.,
12 Mandenius, C.F., Process analytical technology (PAT) for biopharmaceuticals.
13 *Biotechnol J* 6: 369-377 (2011).
- 14 12. Bhambure, R., Kumar, K., Rathore, A.S. 2011. High-throughput process development for
15 biopharmaceutical drug substances. *Trends Biotechnol* 29(3): 127-135.
- 16 13. Smith, D., Process monitoring and control using live cell imaging for the manufacturing
17 of cell therapies. *Doctoral thesis*, Loughborough University (2014).
- 18 14. Ündey, C., Ertunç, S., Mistretta, T., Looze, B., Applied advanced process analytics in
19 biopharmaceutical manufacturing: challenges and prospects in real-time monitoring and
20 control. *J Process Control* 20: 1009-1018 (2010).

- 1 15. Mayer, E., Gardiner, D.J., Hester, R.E., Resonance Raman spectra of vitamin B12 and
2 dicyanocobalamin. *Biochim Biophys Acta* **297**: 568-570 (1973).
- 3 16. Zhang, Z., Wang, B., Yin, Y., Mo, Y., Surface-enhanced Raman spectroscopy of vitamin
4 B12 on silver particles in colloid and in atmosphere. *J Mol Struct* **927**: 88-90. (2009)
- 5 18. Abu Bakar, M.R., Nagy, Z.K., Saleemi, A.N., Rielly, C.D., The impact of direct
6 nucleation control on crystal size distribution in pharmaceutical crystallization processes,
7 *Cryst Growth Des*, **9**:1378-1384 (2009).
- 8 19. Saleemi, A.N., Rielly, C.D., Nagy, Z.K. 2012a, Automated direct nucleation control for in
9 situ dynamic fines removal in batch cooling crystallization, *CrystEngComm*, **14**: 2196-
10 2203 (2012a).
- 11 20. Saleemi, A.N., Rielly, C.D., Nagy, Z.K. 2012b, Comparative investigation of
12 supersaturation and automated direct nucleation control of crystal size distribution using
13 ATR-Uv/Vis spectroscopy and FBRM, *Cryst Growth Des*, **12**: 1792-1807 (2012b).
- 14 21. Saleemi, A.N., Steele, G., Pedge, N.I., Freeman, A., Nagy, Z.K., Enhancing crystalline
15 properties of a cardiovascular active pharmaceutical ingredient using a process analytical
16 technology based crystallization feedback control strategy, *IntJ Pharm*, **430**(1-2): 56-64
17 (2012).
- 18 22. Leyssens, T., Baudry, C., Hernandez, M.L.E., Optimization of a crystallization by online
19 FBRM analysis of needle-shaped crystals. *Org Process Res Dev*, **15**: 413-426 (2011).

20

1 **Table 1: Solubility of vitamin B12 in water at different temperature (data provided by Hebei Welcome**
2 **Pharmaceutical Co., LTD)**

| Temperature (°C) | Solubility (g/l water) |
|-------------------------|-------------------------------|
| 10 | 9.25 |
| 20 | 10 |
| 25 | 11.5 |
| 30 | 13.5 |
| 45 | 24 |

3

4

5

1 **Table 2: Experiment conditions, slow and fast cooling of raw and crystallized material**

| Experiment | Solvent | Vitamin concentration (g/g solvent) | Type of material | Cooling rate (°C/min) | Seeding |
|------------|---------------|--|----------------------------------|------------------------|-------------|
| 1 | Ethanol/water | 0.118 | Raw | -0.5 (fast cooling) | No |
| 2 | Ethanol/water | 0.118 | Raw | -0.1 (slow cooling) | No |
| 3 | Water | 0.097 | Crystallized (more than once) | -0.5 (fast cooling) | No |
| 4 | Water | 0.097 | Crystallized (more than once) | -0.1 (slow cooling) | No |
| 5 | Water | 0.089 | Raw material | -0.1 (slow cooling) | No |
| 6 | Water | 0.106 | Crystallized | -0.075(slower cooling) | No |
| 7 | Water | 0.089 | Raw material | -0.1 (slow cooling) | Yes |
| 8 | Water | 0.097 | Crystallized | -0.1 (slow cooling) | Yes |
| 9 | Ethanol/water | 0.119 | Raw | -1 (faster cooling) | No |
| 10 | Ethanol/water | 0.119 | Raw | -1 (faster cooling) | Yes |
| 11 | Ethanol/water | 0.119 | Raw | -0.5 (fast cooling) | No |
| 12 | Ethanol/water | 0.119 | Raw | -0.5 (fast cooling) | Yes |
| 13 | Ethanol/water | 0.119 | Raw | -0.1 (slow cooling) | No |
| 14 | Ethanol/water | 0.119 | Raw | -0.1 (slow cooling) | Yes |
| 15 | Ethanol/water | 0.13 | Crystallized | -1 (faster cooling) | No |
| 16 | Ethanol/water | 0.13 | Crystallized | -0.5 (fast cooling) | No(150 rpm) |
| 17 | Ethanol/water | 0.13 | Crystallized | -0.5(fast cooling) | No(240rpm) |
| 18 | Ethanol/water | 0.13 | Crystallized | -0.5 (fast cooling) | Yes |
| 19 | Ethanol/water | 0.13 | Crystallized | -0.1 (slow cooling) | No |
| 20 | Ethanol/water | 0.115 | Raw | -0.5 | No |
| 21 | Ethanol/water | 0.137 | From exp. 20 | -0.5 | No |
| 22 | Water | 0.082 | From exp. 21 | -0.5 | No |

2

1

Table 3: HPLC results for selected experiments performed

| Sample | Purity (%) | Improvement in purity (%) | Solvent used | Material used | Cooling rate (°C/min) | Seeded |
|-------------------------|--------------|---------------------------|----------------------|--------------------|-----------------------|------------|
| Raw material | 93.11 | 0 | n.a. | n.a. | n.a. | n.a. |
| First crystallization | 96.14 | 3.03 | n.a. | n.a. | n.a. | n.a. |
| Second crystallization | 97.29 | 1.16 | n.a. | n.a. | n.a. | n.a. |
| Third crystallization | 98.03 | 0.74 | n.a. | n.a. | n.a. | n.a. |
| LC experiment 8 | 97.54 | 1.24 | Water | Crystallized | -0.1 | Yes |
| LC experiment 9 | 96.35 | 3.24 | Ethanol/water | Raw | -1 | No |
| LC experiment 10 | 96.28 | 3.17 | Ethanol/water | Raw | -1 | Yes |
| LC experiment 11 | 96.28 | 3.17 | Ethanol/water | Raw | -0.5 | No |
| LC experiment 12 | 96.72 | 3.61 | Ethanol/water | Raw | -0.5 | Yes |
| LC experiment 13 | 96.51 | 3.40 | Ethanol/water | Raw | -0.1 | No |
| LC experiment 14 | 96.76 | 3.65 | Ethanol/water | Raw | -0.1 | Yes |
| LC experiment 15 | 97.66 | 0.94 | Ethanol/water | Crystallized | -1 | No |
| LC experiment 16 | 97.70 | 0.98 | Ethanol/water | Crystallized | -0.5 | No |
| LC experiment 17 | 97.72 | 1.00 | Ethanol/water | Crystallized | -0.5 | No |
| LC experiment 18 | 97.95 | 1.23 | Ethanol/water | Crystallized | -0.5 | Yes |
| LC experiment 19 | 97.77 | 1.05 | Ethanol/water | Crystallized | -0.1 | No |
| LC experiment 20 | 96.14 | 3.03 | Ethanol/Water | Raw | -0.5 | No |
| LC experiment 21 | 97.29 | 1.16 | Ethanol/Water | Crystallized once | -0.5 | No |
| LC experiment 22 | 98.03 | 0.74 | Water | Crystallized twice | -0.5 | No |

2

3

1 **List of Figures:**

2 **Figure 1:** Molecular structure of cyanocobalamin. The CN group constitutes the difference
3 from the natural vitamin B12 and it is the results of the extraction procedure by which the
4 compound is removed from bacterial cultures.¹

5 **Figure 2:** schematic of the equipment used during the experiments.

6 **Figure 3:** inferential solubility curve expressed as UV signal versus temperature in the two
7 solvents used. The addition of ethanol increased the solubility of vitamin B12 especially at
8 high temperature. This type of curve can replace the classical concentration versus
9 temperature relationship in cases in which only a small amount of material is available and
10 literature data are not available.

11 **Figure 4:** Microscope image of the crystals at the end of experiment 1 (fast cooling) (b)
12 Microscope image of the bigger crystals at the end of experiment 2 (slow cooling) (c)
13 Microscope image of the smaller crystals at the end of the experiment 2.

14 **Figure 5:** (a) Experiment 1: fast cooling of raw material in water and ethanol, $-0.5^{\circ}\text{C}/\text{min}$.
15 The graph shows the total counts per measurement and the mean of the square weighted
16 chord length distribution (MSWCLD) from the FBRM (b) Experiment 2: slow cooling of raw
17 material in water and ethanol, $-0.1^{\circ}\text{C}/\text{min}$. The graph shows the total counts per measurement
18 and the mean of the square weighted chord length distribution from the FBRM (c)
19 Experiment 1: chord length distribution for the fast cooling experiment (d) Experiment 2:
20 chord length distribution for the slow cooling experiment.

21 **Figure 6:** Absorbance value at 361nm, Total counts from FBRM and mean of the square
22 weighted chord length distribution (MSWCLD) for (a) Experiment 3: fast cooling and
23 crystallization of purified material dissolved in water (b) Experiment 3: microscopic image of
24 the final crystals for the fast cooling experiment in water (c) Experiment 4: slow cooling and

1 crystallization of purified material dissolved in water (d) Experiment 4: microscopic image of
2 the final crystals for the slow cooling experiment in water.

3 **Figure 7:** (a) Experiment 3: chord length distribution (CLD) during the fast cooling
4 experiment in water with purified material (b) Experiment 4: chord length distribution (CLD)
5 during the slow cooling experiment in water with purified material.

6 **Figure 8:** (a) Experiment 5: slow cooling $-0.1^{\circ}\text{C}/\text{min}$ of raw material. Total counts per
7 measurement from FBRM and absorbance from ATR-UV/Vis. (b) Experiment 6: slow
8 cooling $-0.075^{\circ}\text{C}/\text{min}$ of recrystallized material. Total counts per second from FBRM
9 (Loughborough University) and UV derivative signal. (c) Experiment 7: seeded and slow
10 cooling of raw material in water ($-0.1^{\circ}\text{C}/\text{min}$) (d) Experiment 8: seeded and slow cooling of
11 recrystallized material in water ($-0.1^{\circ}\text{C}/\text{min}$).

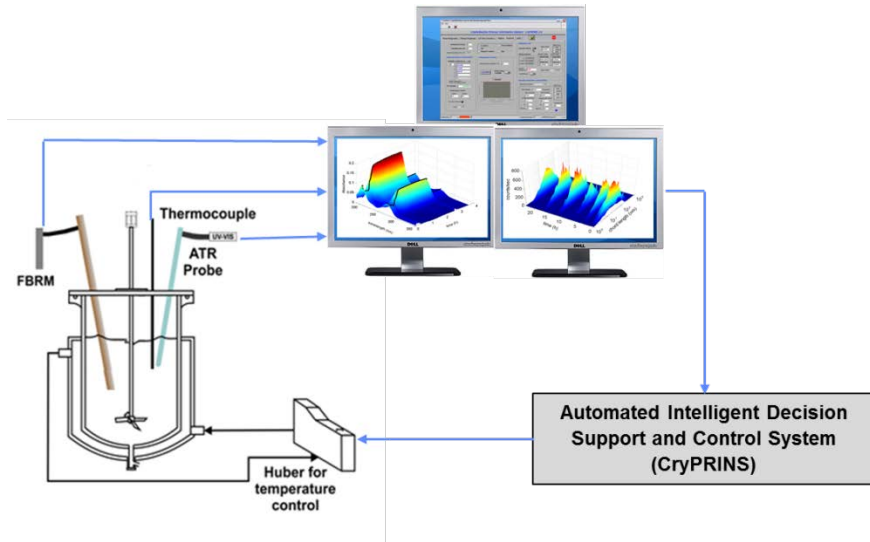
12 **Figure 9:** (a) Chord length distribution (CLD) in the seeded and slow cooling of raw material
13 in water (Experiment 7) (b) Microscopic image of the final crystals for the seeded and slow
14 cooling of raw material in water (Experiment 7).

15 **Figure 10:** (a) Raman spectra of the raw material donated and the particles filtered at high
16 temperature (b) Raman spectra of the crystals from the three consecutive crystallizations. A
17 loss in fluorescence can be noticed.

18 **Figure 11:** (a) Score of the second principal component (PC2) plotted against the first
19 principal component (PC1) for all the samples analysed. (b) Score of the second principal
20 component (PC2) plotted against the first principal component (PC1) for the crystallized
21 samples.

22 **Figure 12:** microscopic images of (a) Raw vitamin B12 from fermentation (b) Crystal
23 obtained after the first crystallization (c) Crystal at the end of the second crystallization (d)
24 Crystals after the third crystallization

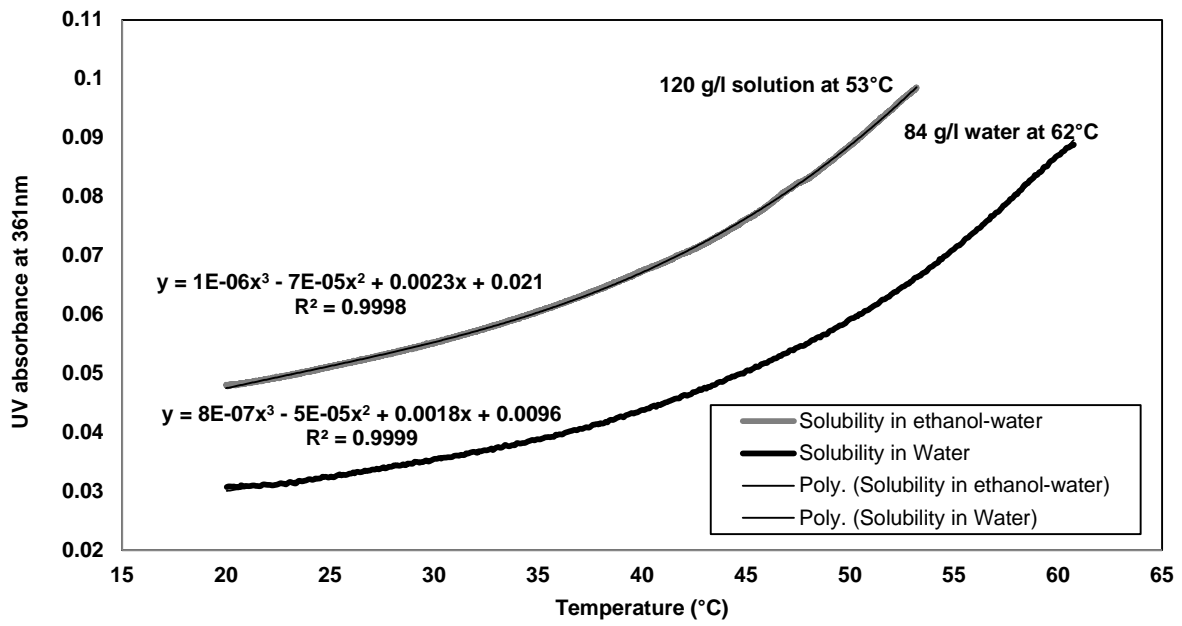
25
26



1

2 **Figure 2: schematic of the equipment used during the experiments.**

3

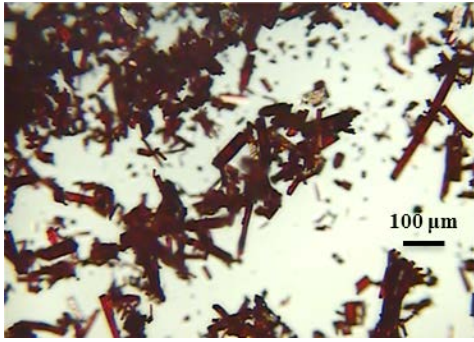


1

2

3 Figure 3: inferential solubility curve expressed as UV signal versus temperature in the two solvents used. The
 4 addition of ethanol increased the solubility of vitamin B12 especially at high temperature. This type of curve can
 5 replace the classical concentration versus temperature relationship in cases in which only a small amount of material
 is available and literature data are not available.

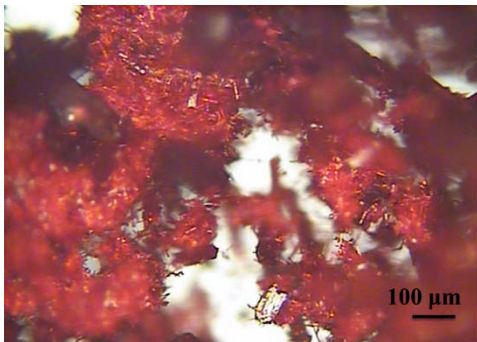
6



(a)



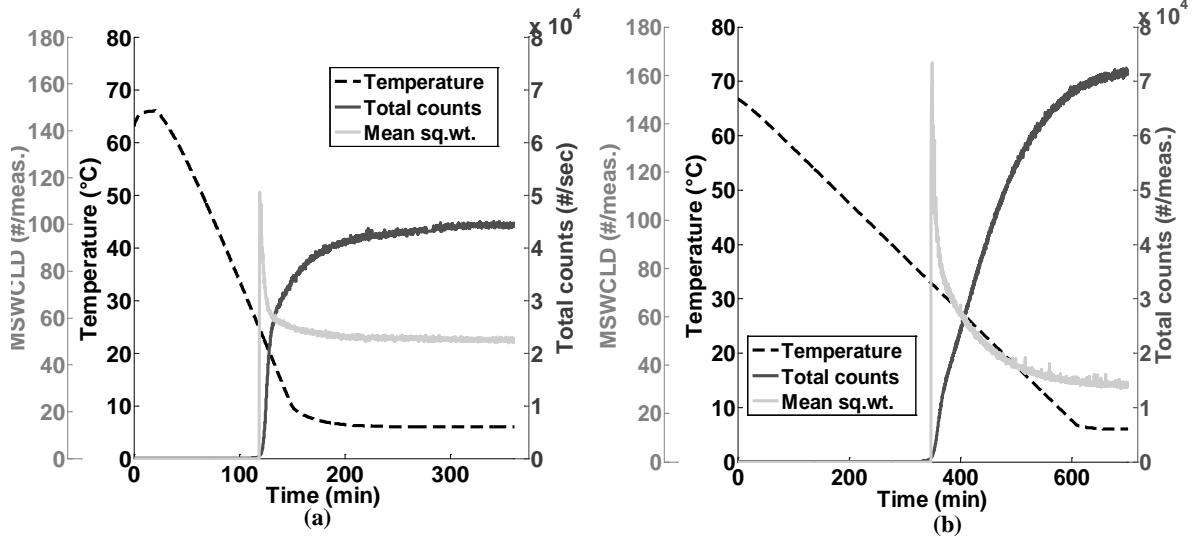
(b)



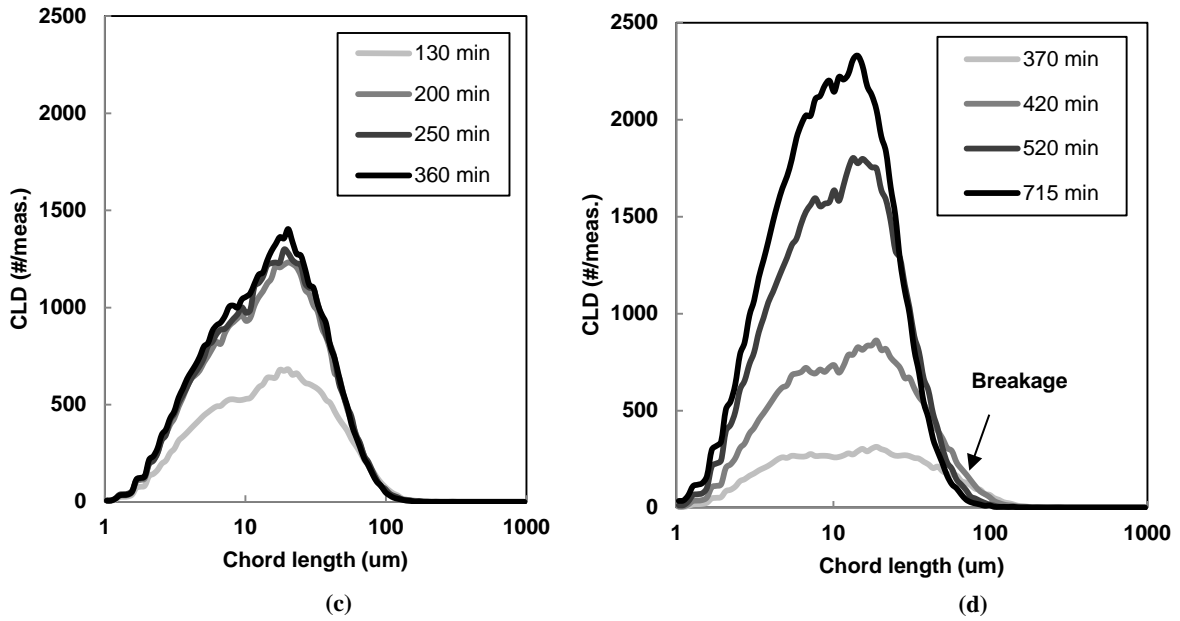
(c)

6 **Figure 4: (a) Microscope image of the crystals at the end of experiment 1 (fast cooling) (b) Microscope image of the**
7 **bigger crystals at the end of experiment 2 (slow cooling) (c) Microscope image of the smaller crystals at the end of the**
8 **experiment 2.**

9



1

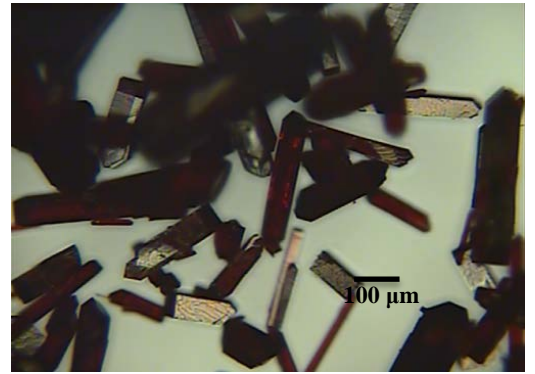
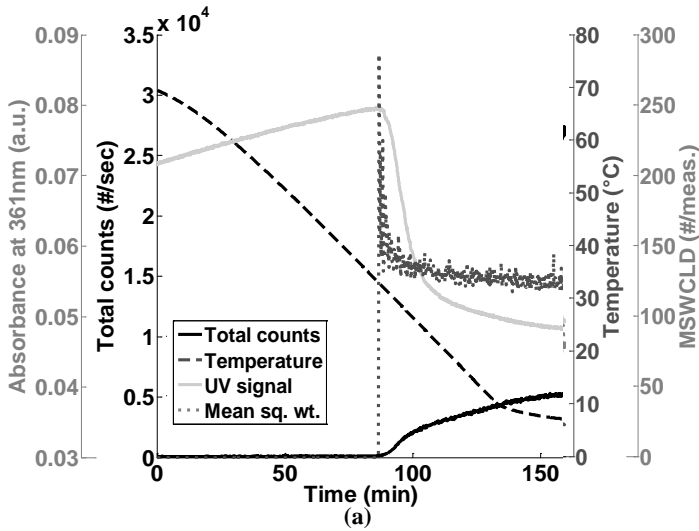


2

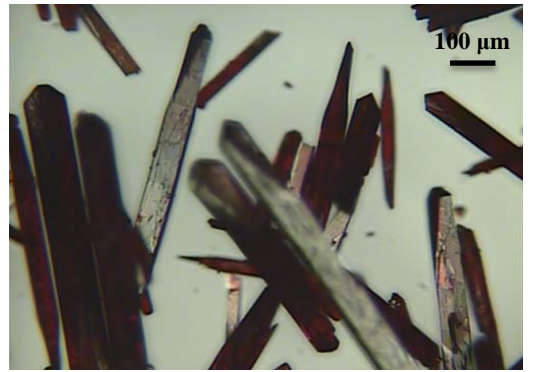
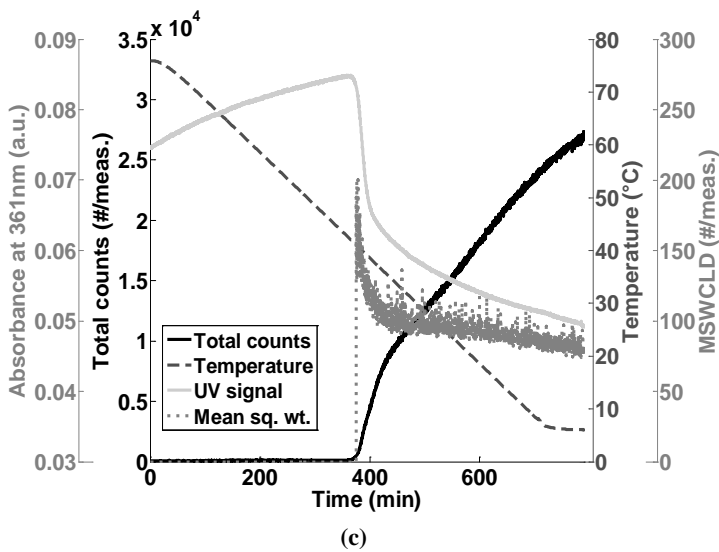
3

4 **Figure 5: (a) Experiment 1: fast cooling of raw material in water and ethanol, -0.5°C/min. The graph shows the total**
 5 **counts per measurement and the mean of the square weighted chord length distribution (MSWCLD) from the FBRM**
 6 **(b) Experiment 2: slow cooling of raw material in water and ethanol, -0.1°C/min. The graph shows the total counts**
 7 **per measurement and the mean of the square weighted chord length distribution (MSWCLD) from the FBRM (c)**
 8 **Experiment 1: chord length distribution (CLD) for the fast cooling experiment (d) Experiment 2: chord length**
 9 **distribution (CLD) for the slow cooling experiment.**

10

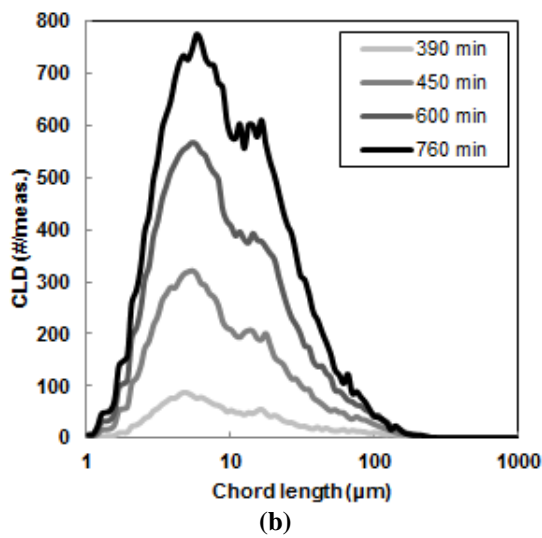
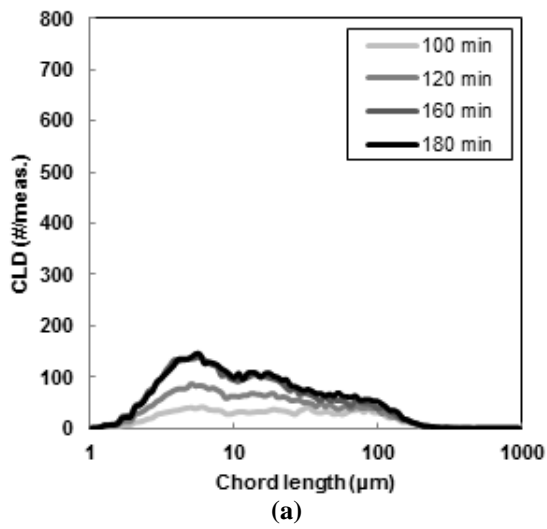


(b)



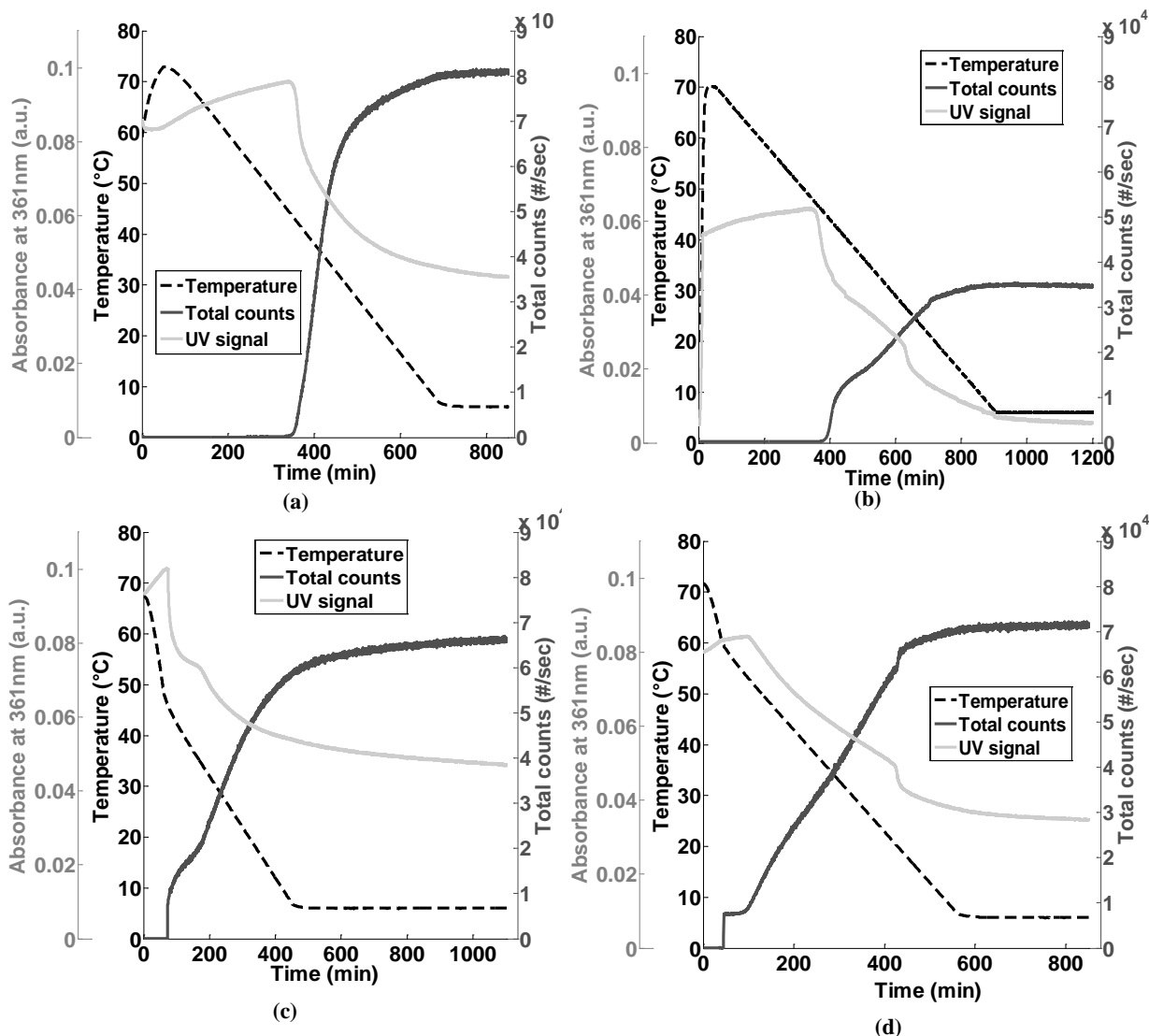
(d)

Figure 6: Absorbance value at 361nm, Total counts from FBRM and mean of the square weighted chord length distribution (MSWCLD) for (a) Experiment 3: fast cooling and crystallization of purified material dissolved in water (b) Experiment 3: microscopic image of the final crystals for the fast cooling experiment in water (c) Experiment 4: slow cooling and crystallization of purified material dissolved in water (d) Experiment 4: microscopic image of the final crystals for the slow cooling experiment in water.



1
2
3
4
5
6

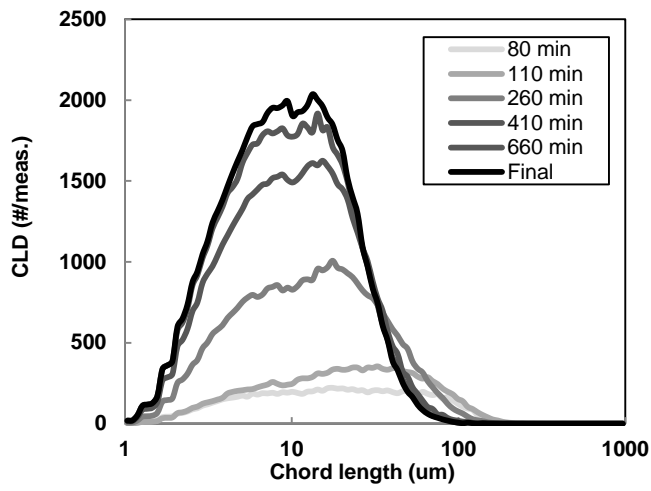
Figure 7: (a) Experiment 3: chord length distribution (CLD) during the fast cooling experiment in water with purified material (b) Experiment 4: chord length distribution (CLD) during the slow cooling experiment in water with purified material.



1
2
3
4
5
6
7
8

Figure 8: (a) Experiment 5: slow cooling $-0.1^{\circ}\text{C}/\text{min}$ of raw material. Total counts per measurement from FBRM and absorbance from ATR-UV/Vis. (b) Experiment 6: slow cooling $-0.075^{\circ}\text{C}/\text{min}$ of recrystallized material. Total counts per second from FBRM (Loughborough University) and UV absorbance. (c) Experiment 7: seeded and slow cooling of raw material in water ($-0.1^{\circ}\text{C}/\text{min}$) (d) Experiment 8: seeded and slow cooling of recrystallized material in water ($-0.1^{\circ}\text{C}/\text{min}$). Total counts per measurement from FBRM and absorbance from ATR-UV/Vis.

1



2

(a)

3

4

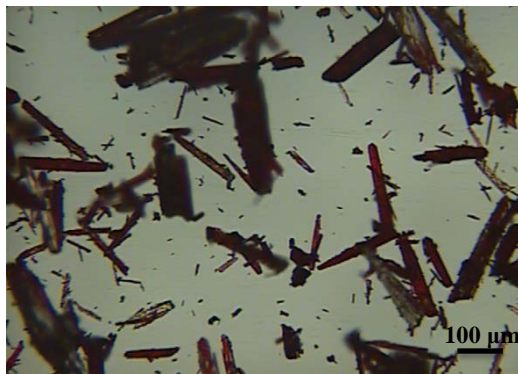
5

6

7

8

9



(b)

10

11

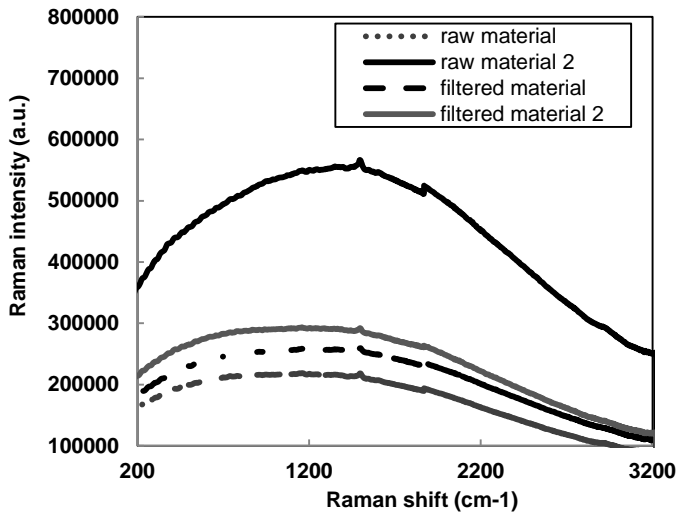
12 **Figure 9: (a) Chord length distribution (CLD) in the seeded and slow cooling of raw material in water (Experiment 7)**

13 **(b) Microscopic image of the final crystals for the seeded and slow cooling of raw material in water (Experiment 7).**

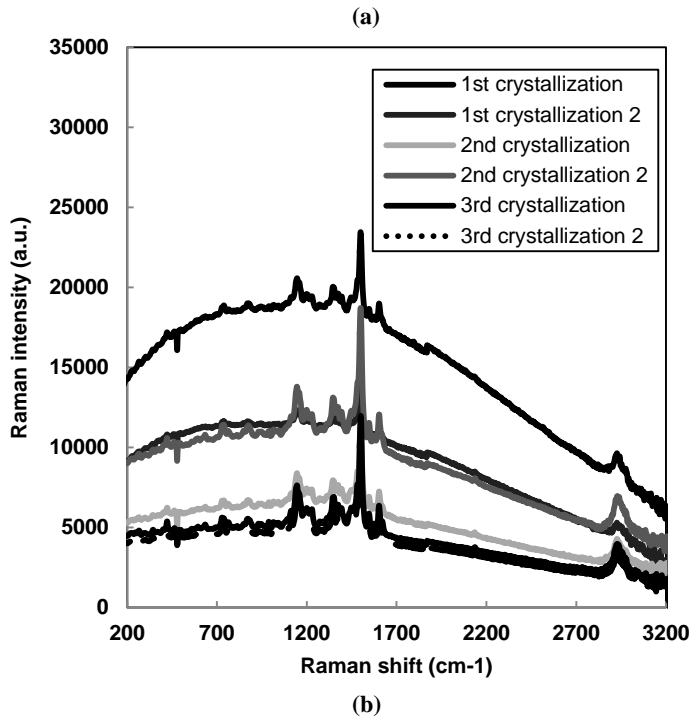
14

15

1



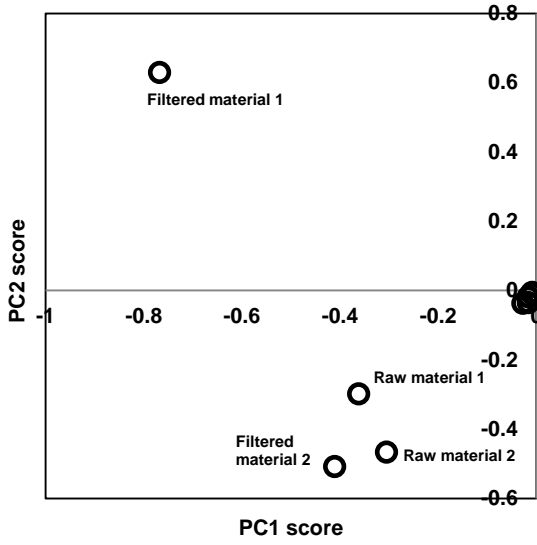
2



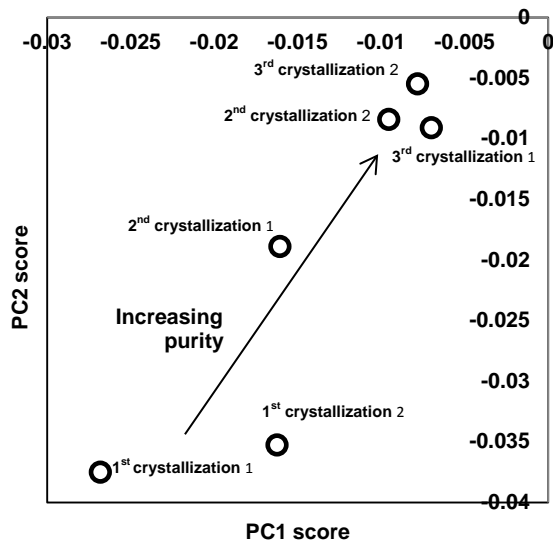
3

4 Figure 10: (a) Raman spectra of the raw material donated and the particles filtered at high temperature (b) Raman
5 spectra of the crystals from the three consecutive crystallizations. A loss in fluorescence can be noticed.

6



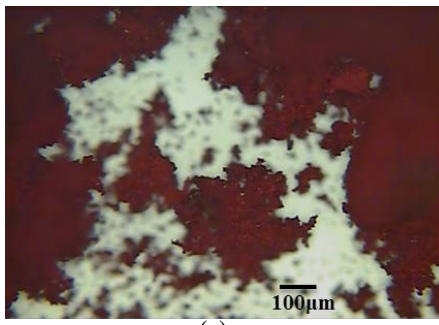
(a)



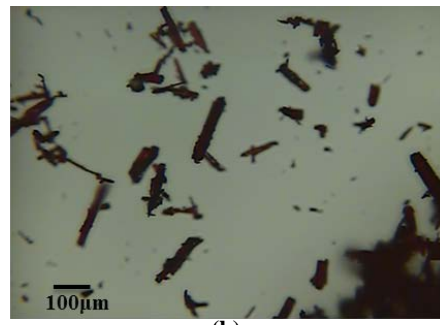
(b)

Figure 11: (a) Score of the second principal component (PC2) plotted against the first principal component (PC1) for all the samples analysed. (b) Score of the second principal component (PC2) plotted against the first principal component (PC1) for the crystallized samples.

1



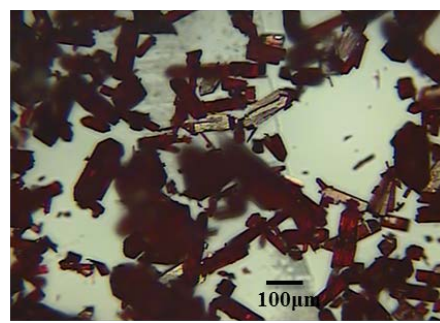
(a)



(b)



(c)



(d)

2

3 **Figure 12: microscopic images of (a) Raw vitamin B12 from fermentation (b) Crystal obtained after the first**
4 **crystallization (c) Crystal at the end of the second crystallization (d) Crystals after the third crystallization**

5

6